Management of secondary effluent using novel membrane technology to recover water and magnesium ions for phosphate precipitation: an integrated pilot-scale study

Anna Bastrzyk[1], Kornelia Pacyna-Iwanicka[1], Anna Dawiec-Liśniewska[2], Krystian Czuba[1,3], Kamil Janiak[3,4] , Przemysław Chrobot[4], Oseweuba Valentine Okoro[5], Amin Shavandi[5], Daria Podstawczyk[1*]*

[1]Department of Process Engineering and Technology of Polymer and Carbon Materials, Faculty of Chemistry, Wroclaw University of Science and Technology, Norwida 4/6, 50-373 Wroclaw, Poland

[2]Department of Advanced Materials Technologies, Faculty of Chemistry, Wroclaw University of Science and Technology, Smoluchowskiego 25, 50-372 Wroclaw, Poland

[3]Department of Water and Wastewater Treatment Technology, Faculty of Environmental Engineering, Wroclaw University of Science and Technology, Norwida 4/6, 50-373 Wroclaw, Poland

[4]Center of New Technologies, Municipal Water and Sewage Company, Na Grobli 19, 50-421 Wroclaw, Poland

[5]BioMatter unit - École Polytechnique de Bruxelles, Université Libre de Bruxelles (ULB), Avenue F.D. Roosevelt, 50 - CP 165/61, 1050 Brussels, Belgium.

[*]daria.podstawczyk@pwr.edu.pl

[*]anna.dawiec@pwr.edu.pl

KEYWORDS: ion exchange, secondary effluent, anaerobic digestion liquor, struvite, magnesium, phosphates.

Abstract:

Phosphorus and magnesium are comprised as essential resources in the European Union's list of critical raw materials. Access to those nutrients together with growing potable water demand is becoming a serious problem. Many efforts have been made to develop effective technologies for recycling water and essential nutrients from wastewater over the past few decades. Here, we present a new approach for the recovery of water simultaneously with the reclamation of Mg^{2+} and phosphates from secondary effluent (SE) and anaerobic digestion liquor (ADL) at WWTPs. Following the circular economy principles, our technology manages SE and produces two important products, (1) pure water (permeates) and (2) Mg-rich concentrates (by-streams/retentates), for further phosphate recovery from ADL in the form of struvite (MAP). The present study proposes an approach of combining energy-saving membrane processes (ultrafiltration (UF) and nanofiltration (NF)) with ionic exchange (IE) with the UF-NF-IE-NF-concentrates serving as a source of Mg^{2+} in struvite (MAP) precipitation from ADL. Different reaction conditions led to the development of typical MAP crystal forms, such as pyramids, needles, and x-shapes. The study also demonstrated that due to the low heavy metal content and narrow size distribution, the MAP generated could also be employed as a fertilizer.

1 Introduction

Circular economy necessitates that waste should be reused and valorised to promote maximum value extraction and also ensure sustainable management of by-products while maintaining low energy and raw material consumption [1,2].

Since water scarcity affects ~ 38% and ~48% of the EU population and global population respectively, significant attention has been given to the development of an efficient, cost-effective and eco-friendly technology to reclaim water from secondary effluent (SE) [3–6]. This SE is generated in situ in WWTPs for multifarious applications in industry, agriculture and elsewhere [3–6].

In our previous study, we demonstrated that multistep membrane processes – such as microfiltration (MF)/ultrafiltration (UF), nanofiltration (NF), and reverse osmosis (RO) – make it possible to reclaim water of various qualities: from cooling water to tap water [3]. These processes produce not only permeate-purified water but also a retentate by-product that is rich in other valuable ingredients. Given that Mg and Ca concentrations in SE are ca. 8-100 mg/L and 48-110 mg/L, while 98% of divalent cations are retained in NF, the retentates may offer a valuable and inexpensive stream for secondary uses such as in phosphorus (P) fertilizer production.

The low quality of agricultural lands (30-40% of the world's cultivated land is deficient in P) and the growing demand for food leads to an excessive application of mineral ~~phosphorus (P)~~-fertilizers; the amount of P-fertilizers used in European Union (EU) countries was 1.2 million tons in 2020, which is 21.9% more than that in 2010 [7]. This increase in annual consumption of fertilizer will gradually lead to the complete depletion of nonrenewable geological sources [8], which is estimated to occur between 50 and 100 years from now [9].

Since raw minerals critical for P- and Mg-fertilizer production in the EU comprises over 90% of the imports, there is a supply risk not only due to their inaccessibility but also due to the commercial policy of the importing country or region. This problem is exacerbated by the when supply chains are severely disrupted as observed during the COVID-19 pandemic or geopolitical challenges, especially those supply chains that are initiated outside the EU. Therefore, the cost of producing P- and Mg-fertilizers is rising drastically, which translates to higher food prices. Due to these challenges, the EU Commission recently designated phosphorous and magnesium as critical raw materials for the EU's industry and economy. These elements have been categorized as essential nutrients to support life, as they are components of the commonly used P fertilizers MAP ($(NH_4)Mg[PO_4]\cdot 6H_2O$) [10].

The current priority is to find cheap and easily accessible sources of phosphorus, nitrogen and magnesium ~~or calcium~~. The cheap raw materials commonly used for P-fertilizer precipitation are agro-industrial wastewater rich in P and N, including dairy wastewater [11], wastewater from fish processing factories [12], pharmaceutical wastewater [13], or wastewater from piggery [14,15] and ADL [16] (**Table S1**). ADL is a liquid byproduct of digestion separation in WWTPs that could be an excellent source of P in the precipitation of P-fertilizer, such as MAP. During anaerobic digestion, large amounts of organic matter are gasified, which leads to a substantial release of soluble phosphorus (up to 60-80% of phosphorus loads in raw wastewater) and a considerable increase in its concentrations [17]. As this stream is recirculated to the wastewater treatment plant inlet and mixed with raw wastewater, phosphorous salt precipitation performs P-resource recovery and lowers the plant's P-loading,

consequently enhancing effluent quality and helping minimize eutrophication. Despite the sufficient P and N content, one major obstacle to achieving easy and inexpensive P-fertilizer production from ADL is the lack of sufficient concentrations of magnesium ~~or calcium~~ [18]. At least a 1:1 Mg:P ratio is needed for MAP precipitation [19]. Typically, the Mg:P molar ratio in ADL does not exceed 0.1:1; hence, MAP precipitation from ADL requires supplementation with stock salts ($MgCl_2$ or $MgCO_3$), which significantly pushes up operating costs [12,20,21]. MAP precipitation can be performed by the employment of low-cost sources of magnesium, such as byproducts of magnesium oxide production, seawater nanofiltration concentrate, bittern solution, and flue-gas desulfurization wastewater from coal-fired power plants [22–26]. In such a case, the plant must have access to these sources, which can be limited by its geolocation. Considering the production of P-fertilizer in a WWTP, it is surprising that SE has not been regarded as a potential source of magnesium ~~or calcium~~ ions.

Within this study, we have developed a novel strategy for both water reclamation and valuable nutrient recycling, such as P and Mg~~, and Ca~~, using streams (SE and ADL) generated in situ in WWTPs. For this purpose, we have proposed a three-stage technology including UF-NF-IE-NF, which yields Mg- and Ca-rich concentrates (retentates) with the simultaneous production of purified water (permeates) from SE. In line with the zero waste principle, the UF-NF-IE-NF concentrates, which are traditionally returned to the main wastewater circuit, and ADL were used as a source of Mg^{2+}, PO_4^{3-} and NH_4^+ ions in phosphate salt precipitation. This study investigated the influence of the PO_4^{3-}:NH_4^+ molar ratio and pH on the degree of conversion, morphology, and mineral composition. To our knowledge, no study has explored the recovery of high-value concentrates from effluent concurrent with the production of purified water; nor has a similar efficient approach to the recovery of Mg-rich SE concentrate as a reactant in phosphate salt precipitation been reported.

2 Materials and methods

2.1 Materials

Sodium hydroxide (granules, p.a.) was purchased from Stanlab (Poland). Hydrochloric acid (~35-38% aqueous solution, p.a.) and sulfuric (VI) acid (aqueous solution, min 95%, p.a.) were obtained from POCH (Poland). Sodium carbonate (powder, p.a.) was acquired from Sigma–Aldrich (Germany) and EUROCHEM BGD (Poland), respectively. 1-Pentanol (aqueous solution, purity) and potassium dihydrogen phosphate (powder, p.a.) were supplied by Chempur (Poland). All reagents were used as received unless otherwise specified.

2.2 Analytical methods (SM)

A description of the analytical methods can be found in the Supplementary Material.

2.3 Raw wastewater

The secondary effluent (SE) resulting from the mechanical-biological treatment of municipal wastewater was sourced from the Wroclaw WWTP, Poland. Concentrate #1 (C1) was the final waste product of SE treatment (retentate), generated by the integrated UF-NF-IE-NF process. Concentrate #2 (C2) was the C1 concentrate after calcium removal through the addition of Na_2CO_3. The anaerobic digester liquor ADL originated from sludge filter presses from the

Wroclaw WWTP, Poland, and served as a source of ammonium and phosphates for precipitation experiments. The compositions of the raw materials are shown in **Table 1.**

Table 1. The average concentration of main nutrients in the SE, ADL, concentrate #1 (C1) and concentrate #2 (C2)

Parameter	Unit	SE	ADL	C1	C2
PO_4^{3-}	mg/L	0.15±0.05	95.5±14.25	0±0	0±0
NH_4^+	mg/L	1.3±0.8	895±2.5	0.072±~~0.012~~ 0.026	0.118±~~0.009~~ 0.035
Mg^{2+}	mg/L	16.0±2.9	4.12±0.45	465±55.5	321±11
Ca^{2+}	mg/L	72.4±3.2	38.9±5.35	940±12.5	10±5

2.4 Preparation of Mg-rich concentrate and purified water

Concentrates with high magnesium ~~and calcium~~ ion concentrations and purified water were produced by the processing of SE from the Wroclaw WWTP, Poland, based on the pilot-scale three-stage technology, as shown in **Figure 1**. In the first stage, the SE was treated in a dead-end UF (DE-UF) (2) (Left inset in **Figure 1**) equipped with a hollow fibre membrane W05-VC (inner diameter 0.8 mm, cut off of 80 kDa, Liqui-Flux Filtration, USA) with an effective filtration area of 8.7 m^2, at an initial pressure of 3 bars to remove suspended solids and reduce turbidity. Next, the UF permeate (3) was concentrated in NF according to a batch concentration configuration on the DK2540C50 membrane (cut off from 150-300 Da, GE Power&Water, USA) (4) with an effective filtration area of 1.6 m^2 (Right inset in **Figure 1**) at 12 bars to achieve a 10-fold reduction in the feed volume, and to produce the concentrated retentate (C0) and Permeate I. The experiments were performed on pilot equipment that permits the batch circulation mode for the recycling of the concentrate to the feed tank (3). Permeate I was collected in a tank (5). C0 was transferred to the feed tank of IE (6), from which it was pumped to the IE column (7), filled with Lewatit S 6328 A anion-exchange resin (Lanxess, Germany) and operated in continuous downflow mode for removal of sulfates. The effluent from the IE (8) was the feed (9) in the third stage, NF (10) at 12 bars with feed recirculation, to produce concentrate #1 (C1) and purified water – Permeate II (11). Calcium ions were recovered in the form of calcium carbonate by adding sodium carbonate in a molar ratio of Na/Ca = 2/1. The precipitate was then separated from the liquid by a filter with a strainer and the filtrate served as concentrate #2 (C2). All experiments were carried out at room temperature (~20°C). Stream samples were collected and analysed at each stage for PO_4^{3-}, NH_4^+, $Mg^{2+,}$ and Ca^{2+} using the LCK cuvette test system (Hach, Poland).

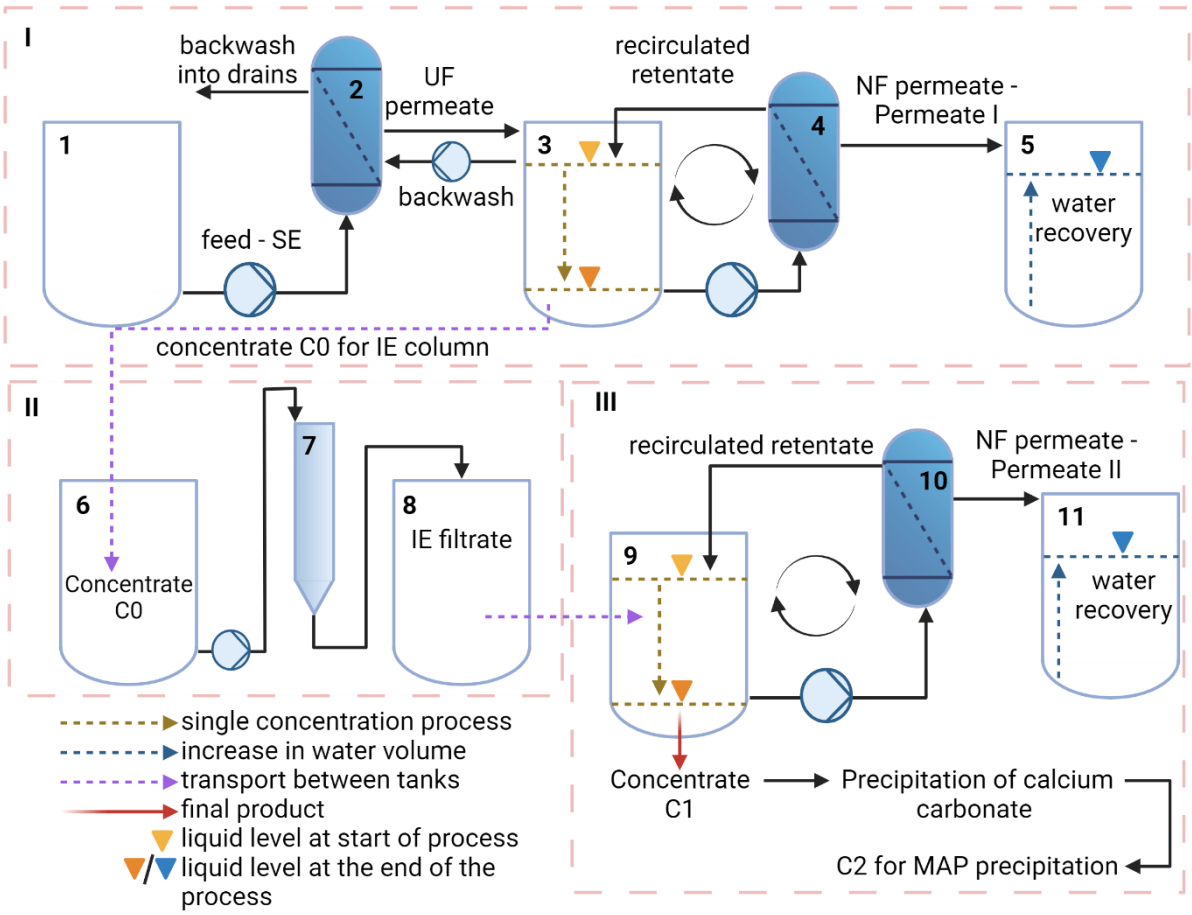

Figure 1. Scheme of the pilot-scale three-stage technology to produce concentrates. Stage I: UF and NF steps: 1 - UF feed tank, 2 - UF membrane module, 3 - UF permeate tank/NF feed tank/NF recirculated retentate tank, 4 - NF membrane module, 5- NF permeate I tank. Stage II: IE: 6 - IE feed tank, 7 - column with IE resin, 8 - IE filtrate tank. Stage III: one more step of NF: 9 - NF feed tank/NF recirculated retentate tank, 10 - NF membrane module, 11 - NF permeate II tank.

MAP precipitation

The MAP precipitation procedure was as follows: initialy, the C2 and ADL were pretreated by filtration for solid removal. Appropriate amounts of C2, ADL, and optionally KH_2PO_4 were subsequently mixed in a jacketed beaker to obtain the final molecular ratio of $Mg/PO_4/NH_4$ or Mg/PO_4 as shown in **Table 2**. Then, the solution pH was then measured and adjusted to the desired value using 0.5 M NaOH or 35-38% HCl. Precipitation was carried out with the following variants: with no agitation and with mixing at ~100 rpm. The duration of the reactions was 2 h. During the reaction, the morphology of the formed crystals was observed under an inverted optical microscope (Leica DMi8, Germany). Precipitated phosphate salts were separated by filtration, washed with water, dried, and stored in a desiccator for further analysis. The concentrations of PO_4^{3-}, NH_4^+, and Mg^{2+} in the supernatant were measured with

Hach's LCK cuvette tests. All experiments were performed at room temperature (20°C). For details, see **Table 2**.

Table 2. Precipitation conditions

GROUP	**I**			**II**		
No.	**1**	**2**	**3**	**4**	**5**	**6**
Source of N, P, and Mg	C2, ADL			C2, ADL, KH_2PO_4		
Molar ratio (Mg^{2+}:PO_4^{3-} :NH_4^+:Ca^{2+})	1:1:20:0.25			1:1:1:0.017		
Mixing rate [rpm]	100	100	0	100	100	0
pH	8.0	9.0	8.0	8.0	9.0	8.0
Reaction Time [h]	2	2	2	2	2	2

The final precipitation test was performed in a thermostated lab-scale reactor (LPP equipment, 20 L) equipped with a motor stirrer, an online pH meter, and a thermostat under reaction conditions (pH, temperature, rate, and time) of test No. 2 and with the reaction volume of 12 L. This experiment aimed to confirm the reproducibility of the results in a higher reaction volume as a preliminary step in process development and scale-up.

2.5 Precipitate characterization

Precipitate characterization methods are described in the Supplementary Material.

3 Results

3.1 Multistage process (UF-NF-IE-NF) to produce water and Mg/Ca-rich concentrates

Our study aimed to recover water and nutrients (Mg ions) from municipal SE in an integrated system combining UF and NF membrane processes and IE. The process was made up of three main stages, each producing water in the form of permeates and/or nutrient-rich retentates, whose quality was assessed. In the first stage, the DE-UF process recovered almost 100% of the SE in the form of permeate while separating mainly suspended solids, which could potentially foul the NF membrane in the next stage of separation. In the following step, the UF permeate-fed the NF with the recirculation mode. The NF process not only retrieved 90% of water (Permeate I) but also produced the intermediate concentrate (C0) by a 10-fold concentration of the retentate/feed volume. After the UF-NF process, the highest retention rates (**Figure 2A**) were achieved for organic compounds, such as COD (97.7±2.9%), total phosphorus (94.7±5.5%), sulfates (90.1±3.8%), and humic substances (87.9±10.6%). Their concentrations reached values of 0.55±0.69 mg/L, 0.009±0.009 mg/L, 13.8±5.3 mg/L, and 0.252±0.078 mg/L, respectively (**Table 3**).

The subsequent IE of C0 removed sulfates, which could affect the ultimate precipitation of phosphate salts. After IE, one more stage of NF was performed, which lead to a total recovery

of 98% of the water from SE (Permeates I+II) and 2% of highly concentrated C1 (retentate). Such recovery efficiency results from the 10-fold reduction in feed volume in the NF and does not include water loss during the operation or maintenance of membrane facilities (e.g. membrane cleaning and backwashing). Typically, these retentates are returned to the main wastewater circuit, affecting the overall pollutant load of wastewater and the performance of the sewage treatment plant.

Table 3. Physicochemical characteristics of permeates after UF-NF (Permeate I) and UF-NF-IE-NF (Permeate II) processes and their combination (I+II). The parameters were evaluated based on the EU Drinking Water Directive 2020/2184s. +/- - complies/does not comply with the requirements of the Directive; N/A - not applicable.

Parameter	Unit	Permeates			Compliment with the potable water standards*		
		I (UF-NF)	II (UF-NF-IE-NF)	I+II (mixed)	I	II	I+II
COD	mg/L	0.55±0.69	4.82±0.23	0.89	N/A	N/A	N/A
P_{total}	mg/L	0.009±0.009	0.011±0.010	0.009	N/A	N/A	N/A
N_{total}	mg/L	8.54±1.32	3.79±1.09	8.16	+**	+**	+**
PO_4^{3-}	mg/L	0.110±0.205	0.095±0.147	0.109	N/A	N/A	N/A
Mg^{2+}	mg/L	2.83±1.72	17.20±6.75	3.98	-	+	-
Ca^{2+}	mg/L	27.9±10.0	106±25	34.1	N/A	N/A	N/A
SO_4^{2-}	mg/L	13.8±5.3	12.1±1.5	13.7	+	+	+
Cl^-	mg/L	184±73	661±117	222	+	-	+
HCO_3^-	mg/L	139±28	169±67	141	N/A	N/A	N/A
HS	mg/L	0.252±0.078	0.238±0.096	0.251	N/A	N/A	N/A
electrical conductivity	µS/cm	1004±115	2144±222	1095	+	+	+
pH	-	7.30±0.37	7.30±0.10	7.30	+	+	+
turbidity	NTU	0.56±0.36	0.22±0.08	0.53	+	+	+
alkalinity	mval/L	2.76±0.77	3.63±0.91	2.83	N/A	N/A	N/A
salinity* (TDS)**	mg/L	702.8	1500.8	766.5	N/A	N/A	N/A

* Based on Polish legislation (consistent with EU directive 2020/2184)

** The maximum nitrate concentration in the potable water is 50 mg/L if the N_{tot} comprises only nitrate, nitrite, and ammonium nitrogen, and if the N_{tot} concentration is <50 mg/L, i.e., the nitrite concentration must also be.

*** Calculated based on the equation reported in [27].

The retention factors after UF-NF-IE-NF were higher than in the first step (UF-NF) and reached values of 97.6±2.2% (P_{total}), 98.5±0.2% (SO_4^{2-}), and 98.3±1.7% (HS). The concentrations of

these compounds were 0.011±0.010 mg/L (P_{total}), 12.1±1.5 mg/L (SO_4^{2-}), and 0.238±0.096 mg/L (HS). The greatest differences can be seen in the retention, concentration of calcium and magnesium cations, and conductivity. The concentration of Ca^{2+} in Permeate I was 27.9±10.0 mg/L with a retention of 75.3±8.9%, while in Permeate II, it was 106±25 mg/L with a comparable retention of 74.8±5.9%. Similarly, Mg^{2+} concentrations were 2.83±1.72 mg/L in Permeate I and 17.20±7.25 mg/L in Permeate II, with retentions of 86.9±8.2% and 87.6±4.1%, respectively. COD retention rates were also close in values in both permeates, 97.7±2.9% and 96.8±2.4%, respectively, while concentrations were 0.55±0.69 mg/L and 4.82±0.23 mg/L. Our technology was highly effective in calcium and magnesium ion separation, fulfilling the purpose of this study. The conductivity of Permeate II (2144±222 µS/cm) was higher – more than twice – than that of Permeate I (1004±115 µS/cm), despite the higher separation of sulfates at the IE stage. The parameters of Permeate II were higher, but considering the small proportion of this stream in the total water recovered, the post-mixed parameters would be similar to those of Permeate I, making it more usable. The mixture of Permeates I and II, in several aspects, meets the standards of various types of water [3].

3.2 Characterization of concentrates

The first stage (UF-NF) simultaneously retained calcium, magnesium, phosphate, and sulfate ions. Through the intermediate IE process, 85% of SO_4^{2-} was removed from concentrate C0. 80% of humic substances (HS) were also separated. Humic acids were found to improve phosphate precipitation [28], but their presence may affect the purity of MAP; hence, they need to be removed. During IE, both compounds were exchanged with chloride ions in the resin, which affected the composition of not only Concentrate C1 but also Permeate II. Chlorides reached a concentration of 184±73 mg/L after UF-NF and increased more than 3 times (661±117 mg/L) when the IE stage was added (UF-NF-IE-NF) (**Table 3**). After IE, the remaining SO_4^{2-} and HS residues were concentrated in the second NF, achieving concentrations of up to 1.1±0.1 (143±18 mg/L) and 5.1±1.0 times (10±2 mg/L), respectively.

The integrated UF-NF-IE-NF process produced a C1 with a high concentration of magnesium and calcium ions. As shown in **Figure 2B**, the ion with the highest concentration factor of 24.0±2.4 is Mg^{2+} with a final concentration of 465±55.5 mg/L (**Table 1**). Ca^{2+} ions were concentrated 13.4±0.6 times, reaching a value of 940±12.5 mg/L (**Table 1**). Compounds that are precursors of struvite were also slightly concentrated: total phosphorus – 1.7±0.1 times while total nitrogen – 1.4±0.3 times; however, their final concentrations remained much lower than those of cations. This result means that precipitation may require an external source of phosphate to achieve the optimal molar ratio of reagents. The calcium ion concentrations in a two-step NF were 3-6 times higher than those in a single-step NF with the same membrane [29]. In contrast, 11-18 times higher magnesium concentrations were obtained, which proves that SE can be completely recycled according to the circular economy concept. Using one source, both water and Ca^{2+}/Mg^{2+}-rich solutions can be produced and reused.

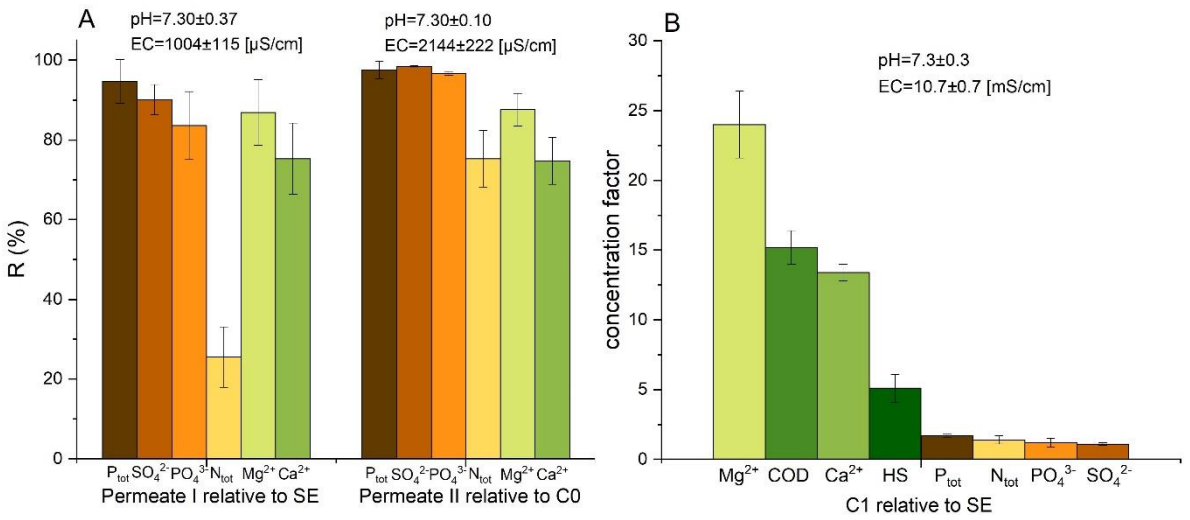

Figure 2. (A) Retention rates (R) of main compounds after UF-NF relative to SE (left) and after UF-NF-IE-NF relative to concentrate C0 (right). NF: 12 bar, DK2540C50 membrane, in circulation mode. IE: Lewatit S 6328A resin, in continuous downflow mode. (B) Concentration factor after UF-NF-IE-NF.

Compared to pure reagents, concentrate C1 shows higher potential to improve the economics and environmental footprint of phosphate recovery in the form of phosphate salts, as C1 is rich in calcium and magnesium ions. As shown in **Table 1**, the concentrations of Mg^{2+} and Ca^{2+} in C1 reached 465 mg/L and 940 mg/L. The circular economy assumptions require that renewable sources of orthophosphates and ammonium ions should also be used. The concentrations of these ions in SE are low because they have to be removed from the wastewater according to standards, hence we sought another stream at the WWTP. ADL was found to be an excellent source of phosphate and ammonium since it is produced in situ at the wastewater treatment plant, and contains ammonium nitrogen and orthophosphate as the main components with concentrations of 895 mg/L and 95.5 mg/L. Because the NH_4^+ level is about 9 times higher than that of PO_4^{3-}, an external source of phosphates might be required to achieve high removal of both species and struvite production yield.

As the high content of calcium ions in C1 could interfere with the crystallization of MAP [30], we reduced Ca ion content to ~15 mg/L. Mg-rich concentrate 2 (C2) was obtained by precipitating Ca^{2+} from C1 as aided by Na_2CO_3. This method is advantageous because, with a well-optimized process, the recovery of calcium in the form of calcium carbonate is almost total with a minor loss of magnesium ions from the solution [31]. The process also recovered 98% (molar basis) of calcium ions in the form of crystalline $CaCO_3$ and eventually produced C2. Calcium carbonate is an additional by-product with a possible application in paper, plastic, paint, or coating industries and agriculture as an additive to pesticides and poultry feed.

3.3 Struvite precipitation and characterization

3.3.1 Group No. I

Next, we perform precipitation experiments to obtain struvite by simply mixing C2 and ADL in an appropriate volume ratio without (Group No. I, samples No. 1-3) and with (Group No. II, Samples No. 4-6) an external source of orthophosphates. Within each group, individual reactions were performed at different initial pHs of 8 (Sample No. 1, 3, 4, and 6) and 9

(Samples No. 2 and 5) and with (Samples No. 1, 2, 4, and 5) and without (Samples No. 3 and 6) stirring.

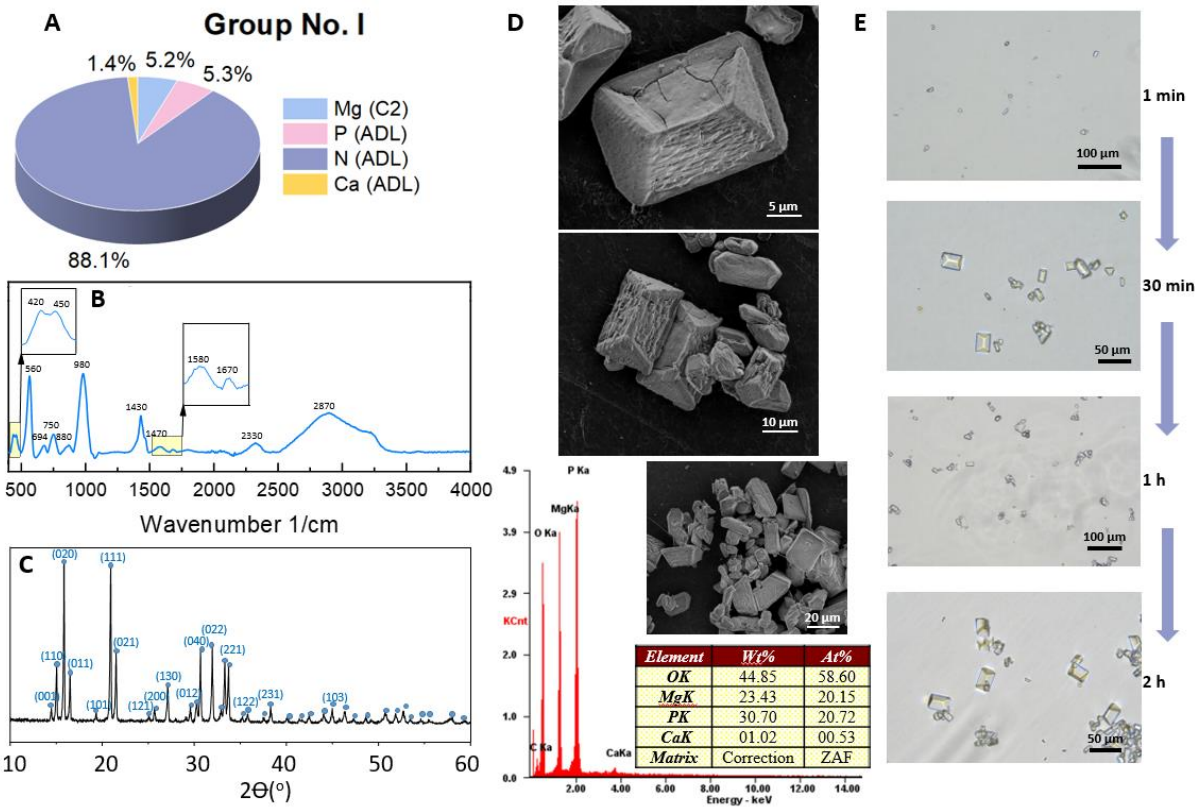

Figure 3. Characterization of phosphate salts from group No. I (**Table 2**, samples No. 1-3) with sample No. 1 as a representative: (A) Pie chart presents the origin and percentage molar contribution of substrates in the precipitation. C2 and ADL were mixed in a proper proportion to achieve the ratio of Mg^{2+}:PO_4^{3-} 1:1; (B) FTIR spectrum of sample No. 1 revealed the functional groups of MAP; (C) XRD pattern of sample No. 1 confirmed the presence of MAP; (D) SEM-EDS micrograph of orthorhombic pyramidal MAP crystals. EDS identified elements such as oxygen, magnesium, calcium, and phosphorus, consistent with the composition of MAP; (E) real-time optical microscopy evaluation of sample No. 1 during a 2-hour experiment. MAP crystals with a hemimorphic structure appeared after 30 minutes of the reaction

In Group No. I (samples No. 1-3), magnesium ions from C2, and ADL as a source of orthophosphates and ammonium were mixed in the volume ratio of ~1/3 to obtain the final ratio of Mg^{2+}/PO_4^{3-} equal 1. As shown in **Figure 3A**, due to the high concentration of NH_4^+ in ADL (895 mg/L), the molar percentage of ammonium ions (88%) far exceeded magnesium (Mg^{2+}) (5.2%) and ortho-phosphates (PO_4^{3-}) (5.3%). The molar ratio of Mg^{2+}:PO_4^{3-}:NH_4^+ was, therefore, 1:1:20. **Table 4** shows that Mg^{2+} and PO_4^{3-} reacted at approximately 58.2% and 50.9%, respectively, while the degree of NH_4^+ conversion was only 0.7% (experiment No. 1). The low recovery of NH_4^+ arises from the 20-fold excess of ammonium ions over those of magnesium and phosphate. In Experiment No. 1, the initial pH was set to 8.0. Based on the research by Hao et al. (2008) [32], we performed precipitation at pH 9 in the next experiment (No. 2) to achieve higher ion conversion degrees. In Experiment No. 2 PO_4^{3-} recovery was 90.4% and Mg^{2+} 76.4% and increased by 39.5% and 18.2%, respectively, compared to the results of No. 1 (**Table 4**). Analysis of the degrees of reaction in experiments No. 1-3 indicates that the precipitated salt corresponds to MAP [33]. When the reaction mixture was not stirred,

the overall reaction performance was lower with only 37.4% and 47.5% conversions of PO_4^{3-} and Mg^{2+}. MAP has been previously precipitated from ADL with additional supplementation of magnesium and phosphate ions in the form of $MgCl_2$ and NaH_2PO_4 salts leading to comparable retention rates of Mg^{2+} and PO_4^{3-} ions at pH 9 (for Mg^{2+}= 70.4% and PO_4^{3-}= 93.9%). Within this study, a higher recovery rate of Mg^{2+} ions and a similar recovery rate of PO_4^{3-} were obtained (PO_4^{3-}= 90.4%, Mg^{2+}= 76.4%) (sample No. 2), which indicates that MAP was effectively precipitated without the addition of any external ingredients. Magnesium, phosphorus, and nitrogen originate from C2 and ADL, which are recovered from WWTP by-streams in accordance with the circular economy paradigm.

Table 4. The conversion degree of NH_4^+, PO_4^{3-}, and Mg^2 species in each process. Source of ~~Ca,~~ Mg, N and P: I – C2, ADL; II – C2, ADL, KH_2PO_4.

			II			III	
No.		**1**	**2**	**3**	**4**	**5**	**6**
Mineral			**MAP**			**MAP**	
Conversion degree [%]	**NH_4^+**	0.7	7.0	0	45.2	55.6	38.2
	PO_4^{3-}	50.9	90.4	37.4	56.8	83.6	49.2
	Mg^{2+}	58.2	76.4	47.5	72.9	84.1	80.3
$pH_{initial}$		8.0	9.0	8.0	8.0	9.0	8.0
pH_{final}		8.1	8.9	8.1	8.1	9.0	8.1
Stirring [rpm]		100	100	0	100	100	0

Next, we used FTIR and XRD analyses to identify the most characteristic functional groups and crystal phases in the precipitated MAP and confirm its presence in the samples. **Figures 3A and 3B** present the XRD and FTIR spectra of sample No. 1, while plots of samples No. 2, and No. 3 are shown in **Figures S2 and S1** in Supplementary Material. All observed diffraction peaks for precipitates No. 1 and No. 3 originating from mixing ADL and C2 in a molar ratio of 1:1:20 (Mg^{2+}:PO_4^{3-}:NH_4^+) were related to MAP, and no impurity phases were found. The presence of MAP in those samples was identified by FTIR analyses. The IR spectra exhibited a major characteristic for the MAP bands at approximately 560 and 980 cm^{-1}, which can be assigned to the antisymmetric bending mode of $v_4(PO_4)$ and the $v_1(PO_4)$ symmetric and $v_3(PO_4)$ antisymmetric stretching mode [34]. The absorption peak at 1430-1470 cm^{-1} was attributed to antisymmetric NH_4^+ bending [35]. The band at 450 cm^{-1} may correspond to Mg-O vibrations or the (PO_4) symmetric bending mode [36]. The characteristic transmission at 2300-2900 cm^{-1} and the slight peaks at 694, 750, and 880 cm^{-1} were related to the H_2O stretching mode and the water vibration mode. These peaks confirmed that the struvite was successfully precipitated.

The efficiency of MAP production and product quality can be enhanced by controlling the precipitation parameters to adjust the size and morphology of the crystals. The shape and size of crystals have a strong impact on the properties of the final product and the efficiency of downstream processes, such as settleability, filtering, and drying [37]. Therefore, to achieve highly effective fertilizer, it is important to determine the dependence of MAP crystal morphology on reaction conditions. Here, the MAP crystal structure was evaluated with optical and scanning electron microscopy. The size of the crystals, including diameter, length, and width, was estimated based on SEM images using ImageJ® according to the protocol proposed by Higgins [38]. Optical and SEM images of the crystals for samples No. 1-6

confirmed the results from the XRD and FTIR measurements. Pure MAP crystals with various morphologies were synthesized as shown in **Figures 3D** and **S3AB**. The samples exhibited a sponge-like internal structure with cracks, fractures, and pores on its surface. Since the reaction substrates originate from wastewater containing numerous organic and inorganic components, such defects may result from the stresses induced by incorporating the other species into the crystal lattice. Another explanation is that irregularities come from the secondary restructuring governed by the Ostwald ripening mechanism [39,40]. MAP crystallized into orthorhombic pyramidal crystals with an average size of 23.29±3.74x14.07±4.80 µm (length x width of the (00$\bar{1}$) face). The crystals consist of {001} pedions, {101} and {012} domes, and {010} pinacoids [41]. A schematic representation of hemimorphic MAP crystals has been demonstrated in several scientific reports [37,41]. The higher ammonium concentrations produced a sharp outcrop of the top (001) face [37] within this hemimorphic structure of MAP. Hemimorphism causes the parallel top (001) and bottom faces (00$\bar{1}$) not to be symmetrically equivalent. When the pH of the reaction mixture was set to 9, MAP crystals developed a rod-like shape (orthorhombic shape) (**Figure S3C**). The irregular surface shown in **Figure 3D** suggests that the crystals had begun to transform into a typical needle-like shape [42] when the reaction was terminated. The crystal-to-crystal transformation phenomenon is even more evident in **Figure S3B**, in which both pyramids and needles are observed. Due to irregular shapes, the actual crystal size was difficult to determine with ImageJ.

Real-time optical microscopy evaluation of sample No. 1 during a 2-hour experiment revealed that tiny MAP crystals (13.99±2.09 µm) were formed immediately after the commencement of the reaction (**Figure 3E**). Subsequently, the crystals quickly (30 min) developed a hemimorphic structure, which remained stable during the total duration of the experiment (2 h). The crystals resembled those visualized by SEM, thereby confirming the presence of orthorhombic pyramidal MAP crystals with an average size of 30.23±6.92x16.44±6.10 µm (length x width of the (00$\bar{1}$) face). After 2 h of the reaction, the pyramids remained stable with an average length of 26.83±6.84 µm. However, needles were also present in the mixture, attesting to the crystal transformation observed in SEM.

3.3.2 Group No. II

In the next stage (Group No. II), to increase the efficiency of nitrogen recovery and the yield of recovered phosphates, an external source of phosphate salt (KH_2PO_4) was added; however, its content did not exceed 31.8% (molar basis)(**Figure 4A**). The initial molar ratio of Mg^{2+}:PO_4^{3-}:NH_4^+ was set to 1:1:1 for experiments No. 4-6. The reaction mixture contained 67.2% (molar basis) of the recycled byproducts generated on the WWTP (C2 and ADL) and only 31.8% of synthetic additives to maintain the optimal molar ratio during MAP precipitation. The system, therefore, is still in line with the idea of the circular economy. The conversion degree of the ions (in experiment No.3, at initial pH 8), was 56.8% for orthophosphate, 45.2% for ammonium nitrogen, and 72.9% for magnesium ions, suggesting the formation of MAP. An increase in the pH value to 9 (No.5) enhanced the recovery of the reagents, in which the degrees of Mg^{2+} and PO_4^{3-} ions concentrations were above 80% (**Table 4**). Unlike in group No. I, when considering the effect of stirring on the reactivity of the ions, we did not observe any change in conversion degrees in sample No. 6 which was similar to that of No. 4. This is in agreement with a previous study [43], in which the stirring had an impact only on the crystal growth rate and not the

efficiency when the molar ratio is 1. It is not, however, valid when ammonium is in excess. Therefore, to ensure homogeneity, mixing of 100 rpm is recommended.

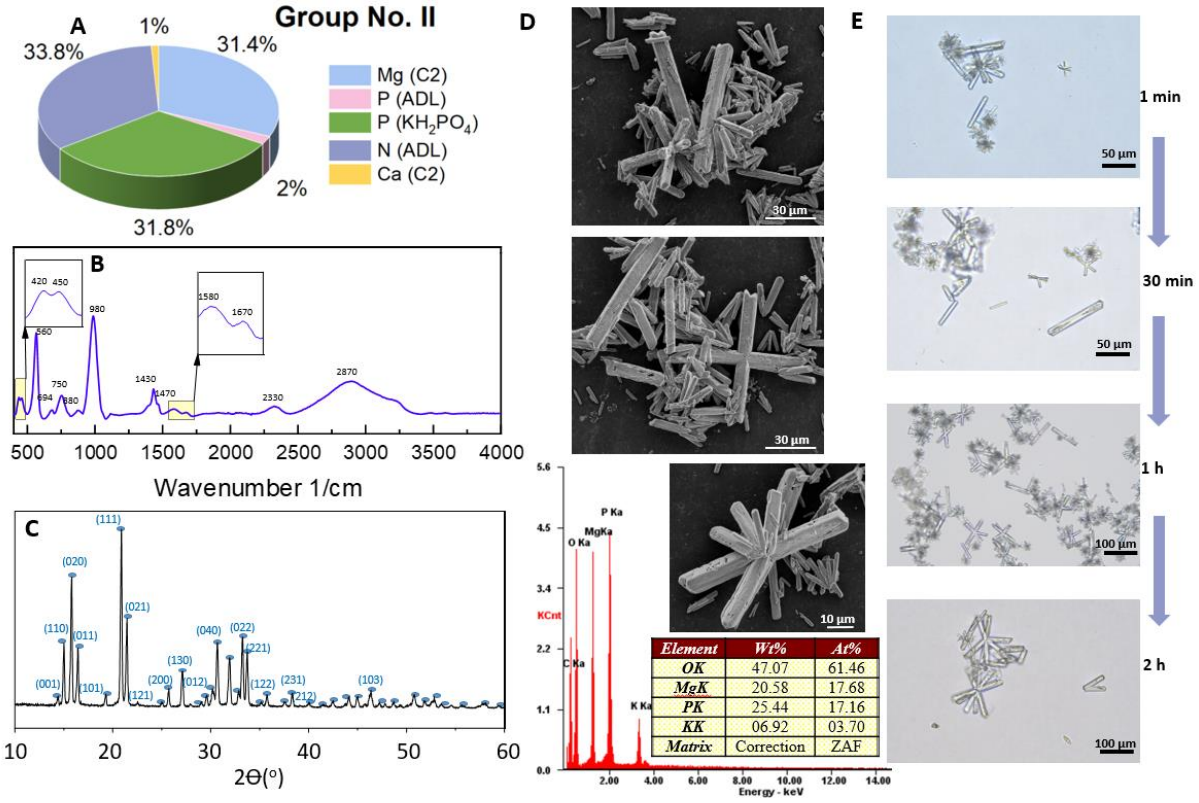

Figure 4. Characterization of phosphate salts from group No. II (**Table 2**, samples No. 4-6) with sample No. 4 as a representative: (A) Pie chart presents the origin and percentage molar contribution of substrates in the precipitation. C2 and ADL were mixed in a proper proportion and an external source of orthophosphates (KH_2PO_4) was added to achieve the ratio of Mg^{2+}:NH_4^+:PO_4^{3-} of 1:1:1; (B) FTIR spectrum of the sample No. 4 revealed the functional groups of MAP; (C) XRD pattern of sample No. 4 confirmed the presence of MAP; (D) SEM-EDS micrograph of MAP with a typical prismatic plate-like shape of crystals elongated in the longitudinal axis. EDS identified elements such as oxygen, magnesium, potassium, and phosphorus, consistent with the composition of MAP; (E) real-time optical microscopy evaluation of sample No. 4 during a 2-hour experiment. MAP crystals with a hemimorphic structure appeared after 1 minute of the reaction

The XRD pattern of sample No. 4 (**Figure 4C**) was compared to that of sample No. 1, and the same peaks were observed at 2θ, corresponding to the characteristic crystal planes of MAP; however, the intensity for the (020) and (022) crystal plane was lower for sample No. 4. This suggests that the MAP crystal growth in sample No. 4 occurs primarily along the (111) crystallographic plane and can exhibit different crystal morphologies than those in sample No. 1. It was previously proved that the crystal lattice structure and crystal defects along with external factors, such as the presence of impurities, and an excess of NH_4^+ ions, can determine the morphology of the MAP crystals [37]. Despite differences in the crystal plane intensities, which can be seen in the XRD patterns of synthesized MAP No. 1 and No. 4, the FTIR spectra of precipitated samples No. 1 - No. 6 were comparable, and no significant shifts were observed (**Figure 6A** and **Figure S2**). FTIR (**Figure 4B**) revealed the functional groups of struvite confirming its presence in samples No. 4-6.

In **Figure 4D**, a typical prismatic plate-like shape of MAP crystals (at pH 8) with a length of 25.99±13.15 µm elongated in the longitudinal axis was identified [44]. In contrast, MAP crystals at pH 9 appeared more rod-shaped with pointed ends (orthorhombic shape) (**Figure S3C**). If the reaction mixture (pH 8) was not subjected to stirring, the needle-like crystals emerged from a mineral center, acquiring a flower-like 3D structure (diameter of 43.69±11.69 µm) (**Figure S3D**). EDS analysis of the precipitates revealed the presence of O, Mg, and P corresponding to the MAP composition. The Mg/P mass ratios of samples No. 1-6 calculated based on the EDS analysis were 0.76±0.05, 0.79±0.04, 0.81±0.02, and 0.83±0.03, respectively, and correspond well (No. 1 and 3) or very well (No. 4 and 5) to the theoretical MAP composition. EDS revealed a trace amount of calcium in MAP samples No. 1 and 3. Minerals No. 4 and 5 contained relatively high amounts of potassium (7.28±0.58 Wt% and 5.52±0.42 Wt%, respectively) that originated in the wastewater streams. This result may suggest that K^+ competes with ammonium ions for phosphates and precipitates as potassium MAP ($KMgPO_4 \cdot 6H_2O$) from the solution containing an equimolar ratio of NH_4^+, PO_4^{3-}, and Mg^{2+}. Therefore, the crystals observed in **Figures 4 and S3D** are a mixture of potassium and ammonium MAP salts.

Crystals of sample No. 4 identified in **Figure 4E** correspond to those visualized in SEM images (**Figure 4D**). Urchin-like crystals with an average size of 42.33±21.32 µm appeared in the system within 1 min of the initiation of the reaction and then grew until they reached 63.15±10.70 µm after 2 h. After 2 h, needle-like crystals began to transform into x-like and twin shapes with an average length of 49.06±11.30 µm.

3.3.3 *Reproducibility of the process*

The controlled struvite precipitation process was performed via crystallization in a thermostated batch reactor (**Figure 5A**) without any external additives (reaction conditions of test No. 2) and recovered phosphates at a rate of almost 75% from ADL (**Figure 5B**). Simultaneously, this system reduced ammonia concentrations by 18%, and more than 90% of Mg^{2+} was consumed from C2 (**Figure 5B**). Even calcium ions were reduced by almost 25%, probably due to the local changes in the alkalinity of the mixture during the reaction, which favors the formation of calcium carbonate [45]. However, the initial number of Ca^{2+} moles is much lower than that of magnesium, ammonium, and phosphate species, which suggests that its presence could be neglected. Insets in **Figure 5B** show the optical images of the crystals that precipitated during the reaction. Struvite-like crystalline forms (needles) appeared within 30 min of the reaction and remained stable until the end of the process (120 min). The change in the numbers of moles of magnesium and ammonium confirms this observation since they reached a constant value within 30 min of the reaction. The experiment confirmed the reproducibility of the process in a higher-volume reactor and is a solid base for technology scale-up. Achieving scalability necessitates addressing the remaining unreacted concentrates. Significantly, no additional chemicals were used for precipitation. This allows the residual

concentrates to seamlessly reintegrate into the main stream, ensuring no discernible increase in the overall load.

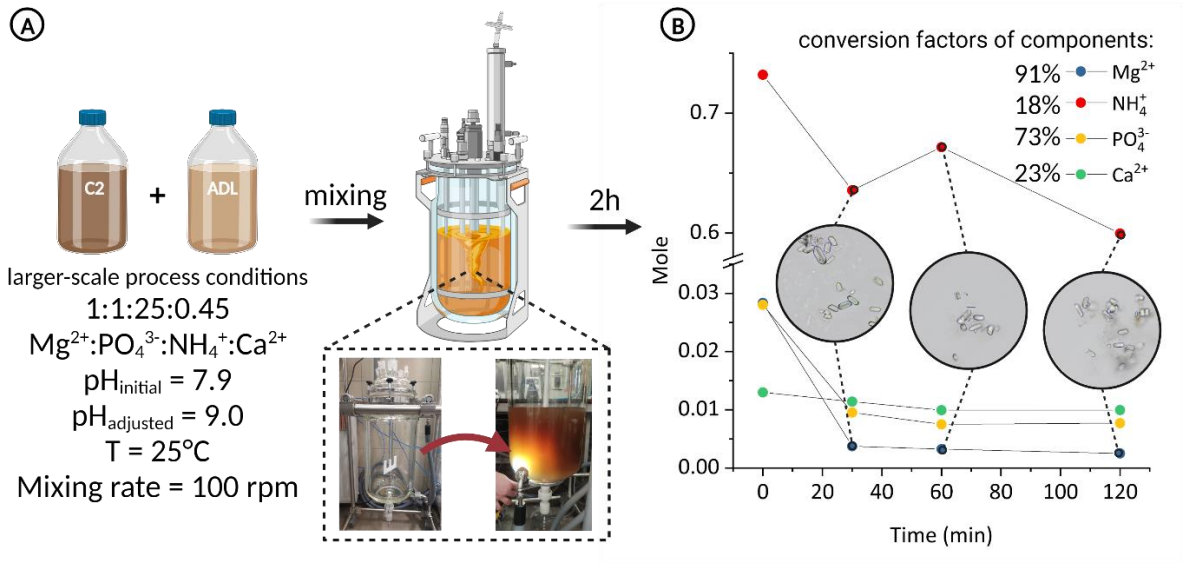

Figure 5. The precipitation test with conditions of experiment No. 2 was performed in a thermostated reactor with a reaction volume of 12 L. (A) Schematic representation of the precipitation test with process conditions and photos (inset) of the empty (left) and filled with reaction mixture (B) reactor; (B) Plot of reaction kinetics (number of reagents moles vs. time).

3.3.4 Quality of the MAP

Crystal size distribution (CSD) and ICP instrumental analyses were used to determine the quality of the precipitated MAP in sample No. 4 (**Figure S4**). As shown in **Figure S4**, 50% of the MAP crystals had an average diameter (d_{50}) of 20.44±0.33 µm. Comparable values were estimated with the aid of SEM images and ImageJ® (**Figure 3D**), where the average length of prismatic plate-like MAP crystals was 25.99±13.15 µm. Crystals with a diameter below 5.39±0.26 µm were marked in less than 10% (d_{10}) in sample No. 4 and may correspond mainly to MAP crystallization nuclei. However, 90% of all MAP crystals were no larger than 52.37±0.67 µm. The average crystal size of MAP produced by means of pure reagents is within the range of 40-60 µm. The size of the crystals precipitated using real reject water instead of pure reagents, was significantly smaller [46]. This phenomenon arises from the presence of suspended solids or organic and inorganic impurities in real WWTP by-streams, which may act as nucleation sites, may reduce, or block active growth sites on the surface of the crystals [47].

Table 5. Content of heavy metals in MAP No. 4 (source Regulation (EU) 2019/1009 of the European Parliament and of the Council of 5 June 2019 established rules to make EU fertilizing products available on the market and amended Regulations (EC) No 1069/2009 and (EC) No 1107/2009 and repealed Regulation (EC) No 2003/2003). DS – dry solids.

Element	Precipitate	Regulation	Element	Precipitate	Regulation
Cd	< 0.5 mg/kg DS	3mg/kg DS	**Pb**	< 0.5 mg/kg DS	120 mg/kg DS
Cr (VI)	< 5 mg/kg DS	2 mg/kg DS	**As**	< 0.5 mg/kg DS	40 mg/kg DS
Hg	< 0.5 mg/kg DS	1mg/kg DS	**Cu**	< 0.5 mg/kg DS	300 mg/kg DS

Ni	< 0.5 mg/kg DS	100mg/k DS	**Zn**	91±31	800 mg/kg DS

In addition to the size of the crystals, it is also necessary to analyse the purity of the obtained salts, especially in the context of the presence of heavy metals. The content of these elements in MAP precipitated from waste is among the most important concerns for its utilization as fertilizer. **Table 5** presents the concentrations of heavy metals, such as cadmium (Cd), hexavalent chromium (Cr VI), mercury (Hg), nickel (Ni), lead (Pb), and arsenic (As), in precipitate No. 4, and the limits of these elements specified in the EU regulations (Regulation (EU) 2019/1009 of the European Parliament and of the Council of 5 June 2019) established rules to make EU fertilizing products available on the market and to amend Regulations (EC) No 1069/2009 and (EC) No 1107/2009 and repeal Regulation (EC) No 2003/2003). EU regulations stipulate that the concentrations of As, Ni, and Pb must not exceed 40, 100, and 120 mg/kg DS, while Hg, Cr(VI), and Cd, which may pose a greater risk to animal or human health, their maximum content in DS must not exceed 1 mg/kg 2 mg/kg and 3 mg/kg, respectively. ICP analysis of sample No. 4 (**Table 5**) shows that the concentrations of all heavy metals were below the detection limit, specified as 0.5 mg/kg DS; except for Cr, which is listed in the EU regulations as an ion (Cr (VI)) and not an element like the rest. Our study also dealt with total chromium (*Cr). The total chromium is composed of both Cr(VI) and Cr(III), as shown in **Table 5.** The Cr concentration in the precipitate was below 5 mg/kg DS. Unlike Cr(VI), Cr(III) is not carcinogenic; rather, it is an important microelement for humans, animals, and plants [48], [49]. Moreover, the uncertainty of measurement at the limit of quantification is predominantly higher; therefore, hexavalent chromium is compliant with EU regulations. As detailed in **Table 5,** following EU regulations, the maximum permissible concentrations of the micronutrients copper (Cu) and zinc (Zn) are 300 mg/kg and 800 mg/kg, respectively. In the precipitated MAP, the amount of Cu was fund to be below the detection limit of 0.5 mg/kg and Zn was 91 mg/kg DS. The zinc content in dry matter positively affects the use of precipitate No. 4 as a fertilizer additive, as Zn influences nitrogen metabolism, photosynthesis, and plant growth processes [50].

4 Discussion

In this study, we selected energy-saving membrane processes (ultrafiltration (UF) and nanofiltration (NF)) with ionic exchange (IE) as a system that valorizes secondary effluent to recover value-added products towards the circular economy. This study may be the foundation to transform wastewater treatment plants into resource recovery facilities.

Secondary effluent contains valuable components, e.g., water as well as calcium and magnesium ions which are usually lost when discharged to surface waters. Our system based on nanofiltration with recirculation enables the concentration of those nutrients and the simultaneous recovery of a high volume of purified water. Recirculation mode, however, may pose a risk of membrane fouling and scaling, thereby decreasing overall NF separation performance. Those phenomena are typically prevented by antiscalants. Most anti-scaling agents inhibit carbonate, phosphate, and sulfate crystallization and are not effective in fouling reduction. Since the antiscalant mechanism is believed to inhibit mineral nuclei formation and delay crystal growth [51,52], its presence in C2 during precipitation could block MAP crystallization. Therefore, antiscalants were not applied in this study. In our previous work, we showed that proper pretreatment through ultrafiltration enables the successful long-term performance of the NF membrane [3]. Here, UF was used to remove suspended solids which

could foul the NF membrane in the next stage of SE separation. UF-NF recovered ~90% of purified water as a permeate I and produced 10-time concentrated retentate (C0). C0 was enriched not only with cations but also with sulfates and humic acids, which could affect the ultimate precipitation of MAP [53]. To limit the addition of chemicals, we used IE to remove those anions. Moreover, thanks to this, IE filtrate free of scalling anions could be further concentrated to recover purified water (98%) and produce much smaller volume of Ca/Mg-rich C1 (2%).

Purified water (Permeates I and II) meets the standards of various types of water, as presented in our previous study [26], and hence can be used as a technological medium in several processes at WWTPs and for agricultural and industrial applications. Additionally, in several aspects, permeate conforms to the drinking water standards. In our previous paper [26], we demonstrated that commonly used disinfection processes, such as UV254, together with chlorination [29], treat NF permeates to have the microbiological water quality and reduce ammonia below the tolerable limits. Therefore, the integration of an additional disinfection step could purify the permeates to the level of safe drinking water. Softened water was obtained because of the high retention rates of magnesium and calcium ions, which could be used in the industry for heating and cooling, as a solvent, as water for cleaning or firefighting, or as an easy-to-manage source of potable water [30].

Next, we managed the byproduct of water reclamation, Ca/Mg-rich (C1) concentrate as a recycled reagent in MAP precipitation. We focused on MAP production since it is a desirable fertilizer for plant growth as it slowly releases micronutrients, such as N and Mg [54–56]. To reduce the number of synthetic reagents, we used ADL, another byproduct from a wastewater treatment plant, as a source of ammonium and phosphate ions (**Table 1**). The exploitation of these two byproducts (concentrates and ADL) in the production of MAP is highly promising. However, acquisition of this mineral is strictly dependent on process conditions, such as the reagent molar ratio and pH. The molar ratio of Ca/Mg plays an important role in precipitation. Ca^{2+} ions inhibit the formation of MAP crystals when Ca/Mg is above 1 because phosphate ions have a higher affinity for Ca^{2+} than Mg^{2+} [57–59]. Literature data show that to form MAP in a system with a higher content of Ca^{2+} than Mg^{2+}, it is necessary to add more magnesium ions as an external source ($MgCl_2$) to lower the Ca/Mg molar ratio below 1 [60]. This does not, however, guarantee the production of a pure product, as it results in the coprecipitation of several phases. At a Ca/Mg molar ratio of 0.5, both the MAP and amorphous phases coexist in the system [57]. In turn, Crutchik and Garrido (2011) [12], to obtain pure MAP in a system containing Ca^{2+}, increased the molar ratio of NH_4^+:PO_4^{3-} from 1 to 4.7, but the molar ratio of Ca/Mg remained below 1. Neither of these solutions is satisfactory, as both require additional supplementation of phosphate ions as well as magnesium and ammonium ions. Our goal was to use the smallest possible amount of external synthetic reagents to maintain the appropriate molar ratio of crystal lattice components; thus, MAP would be obtained and the reaction efficiency would be improved. Therefore, to recover all the valuable nutrients in the form of pure MAP from concentrate and ADL, calcium ions were recovered from C1 by adding sodium carbonate. As a result, C2, which was poor in Ca was yielded. Thus, the recovery of ions, such as magnesium, phosphate, and ammonium, was successful without the addition of external reagents (experiment No. 1-3, **Table 4**) or with a slight supplementation of phosphate ions (37%) (experiments No. 4-6 in **Table 4**). MAP precipitates under alkaline conditions (pH above 7), in which its solubility decreases and reaches a minimum at pH 9 [61]. Thus, to recover valuable nutrients in the form of MAP, we increased the pH of the reaction mixture to 8.0 and

9.0. When the pH of the reaction solution is more alkaline, the phosphate ion recovery increases significantly due to the higher concentration of the HPO_4^{2-} ion, which promotes the formation of Mg-bearing phosphate salts [62]. The recovery of Ca^{2+} ions by calcium carbonate precipitation lowered the Ca/Mg molar ratio to 0.017 (No. 4) and 0.25 (No. 1). In these conditions, with a low amount of interfering Ca^{2+} ions, magnesium ions could interact effectively with ammonium and phosphate ions to form MAP nuclei that could further be combined in surface-mediated dissolution-reprecipitation reactions followed by aggregation, leading to the formation of pure x-like MAP (**Figures 3D and 4D**). This leads to a reduction in the number of crystals (**Figure 4D**) and an increase in crystal diameter up to 49.06±11.30 µm.

In congruence with mass transfer, the growth rate of crystals increases with increasing concentration driving force, and the crystals grow due to the following major steps: (1) transport of the solute from the bulk of the solution to the crystal surface-liquid interface, and (2) surface integration or accumulation of the solute molecules in the layers of the growing crystal. Consequently, the higher the concentration of the crystal lattice ions is, the faster the crystals reach equilibrium and, as a result, differ in size and morphology. MAP crystals that develop more slowly tend to be more tubular or prismatic due to more balanced growth along all the crystal axes [63]. While growing rapidly, MAP crystals are typically dendrimeric and X-shaped because of preferential growth along one crystal axis [63]. In our studies, despite the same molar ratio of Mg^{2+}:NH_4^+:PO_4^{3-}, the amount of the ions of MAP lattice crystals (PO_4^{3-} and Mg^{2+}) in moles was twice as low that in reaction mixture No. 1 (Group No. I) than in system No. 4 (Group No. II). As a result, the crystals grow slower in sample No. 1 than in No. 4 (**Figure 4D**). Even an excess of ammonium ions (x20) in system No. 1 (**Table 2**) did not favour crystal growth because the content of the rest of the lattice crystal ions was significantly lower (**Table 2**) compared to that of reaction No. 4. Furthermore, in reaction mixture No. 1, the organic impurities and other interfering ions such as Ca^{2+} (which greater than in system No. 4 by 10-fold, **Table 2**) can more strongly affect not only the nucleation but also the MAP crystal growth stages compared to system No. 4. This is because the amount of these impurities in relation to the content of Mg^{2+} and PO_4^{3-} in reaction No. 1 was greater than that in reaction No. 4. Organic compounds (from C2 and ADL, **Table 1**) that possess functional groups, such as carboxylic, phenolic, carbonyl, and hydroxyl groups, can form complexes with free Mg^{2+} ions (lowering the access of these ions for phosphates), and adsorb at active sites of the formed crystals, which blocks crystal growth [64–66]. In turn, Ca^{2+} ions can also gather close to the solid-liquid interface and form complexes on the newly formed crystals. This affects the solid-liquid mediated processes during Ostwald ripening and finally slows MAP crystal growth. As a result, in system No. 1, tubular and pyramidal crystals of MAP formed. Regarding the effect of mixing on MAP precipitation (No. 1-6), we observed that smaller crystals formed in the system with agitation (No. 1 and 4) than in the system without mixing (No. 3 and 6). This occurs because the magnetic stirrer exhibits an abrasive or grinding impact, that impedes the formation of a higher number of smaller crystals in the solution [67].

Finally, we assessed the quality of our struvite crystals by analyzing the heavy metal content and CSD in the final product. The impurity level is a especially critical factor determining the usability of MAP as a fertilizer. Recovered streams of natural sources widely employed for MAP production usually come with contaminants (e.g. heavy metals and organic matter) which may co-precipitate or co-exist with MAP, decreasing the overall quality of the fertilizer [68,69]. Limited research focuses on the impurity content in the final crystals since its minimization requires the pre-removal steps such as chemical precipitation [70]. As evidenced

by ICP-OES, we successfully produced highly purified MAP crystals with a low heavy metal degree, which follows the EU regulation No. 2019/1009 establishing rules to make EU fertilizing products available on the market. EDS also confirmed that the only non-struvite components in our samples are calcium (~1 wt.%) and potassium (~7wt.%) with remaining 99 and 93 wt.% of pure MAP.
The CSD is an important feature of MAP since it dictates its applicability e.g. in agriculture as a cheap fertilizer. Larger crystals are slightly more favorable in industrial production due to faster sedimentation and easier post-handling steps. Smaller crystals have a greater release rate of nutrients due to their higher surface area [37]. Our MAP crystals had relatively small size, but narrow CSD which is preferable for further post-processing, e.g. granulation [71].

5 Conclusions

To meet the challenge of circular economy in WWTP, within this study, we present a hybrid membrane-based technology for SE recycling to produce (1) purified water (permeates), and (2) macronutrient-rich concentrates (retentates) as reagents in MAP precipitation from ADL.

We are likely the first to have demonstrated that SE can be a source of clean water and valuable microelements (magnesium ions) for phosphorus recovery from ADL as struvite. Our membrane-based technology (UF-NF-IE-NF) led to the total recovery of 98% of the water from SE as permeates and 2% of highly concentrated Ca^{2+}/Mg^{2+}-rich concentrates (C1/C2) as retentates. Recovered water (permeates) meets the standards of various types of water; hence, can be used as a technological medium in several processes at WWTPs and for agricultural and industrial applications. Additionally, reclaimed water may achieve the drinking water standards, after undergoing disinfection, such as UV_{254}, together with chlorination to conform to the microbiological water quality and reduce ammonia below the tolerable limits.

The results showed that the UF-NF-IE-NF process was capable of concentrating magnesium and calcium ions in retentates by ~30 and ~13 times, respectively. The multistep configuration of the operations was necessary to efficiently remove main impurities, such as solids and sulfates that could adversely affect phosphate precipitation along with final product purity and quality. The final Mg^{2+} concentration in C1 was sufficient to begin precipitation tests of phosphate salts.

In the MAP formation procedure, it was necessary to sequester Ca^{2+} from the concentrates by adding sodium carbonate solution to precipitate $CaCO_3$. Reaction conditions affected the size and morphology of MAP crystals, leading to the development of typical MAP crystal forms, such as pyramids, needles, and x-shapes. XRD confirmed the high crystallinity of the final product. Our approach was reproducible and led to the production of MAP with a narrow crystal size distribution. The final product had high purity as evidenced by the lack of heavy metals embedded within the crystal structure or adsorbed on its surface. We showed that the appropriate selection of process conditions enables a high degree of phosphate removal (>90%), completely dispensing with additives. Still, the addition of an external source of phosphate is recommended to obtain a higher yield of MAP production.

Our results demonstrated that the Mg-rich concentrate provides an opportunity for MAP formation by adapting problematic byproducts, such as retentates, from water reclamation and ADL. The recycling and management of the produced by-streams may close the water

loop in WWTP in conformity with the zero waste concept. Reclaimed water could meet cooling water standards, and the byproduct can be recycled to produce valuable magnesium (struvite) phosphate salts that could be beneficially reused in agriculture.

Our future study will include a comprehensive assessment of the economic feasibility of our proposed process. This assessment will encompass the evaluation of costs, potential economic benefits, and feasibility considerations, aimed at ensuring the readiness of the process for scaling up. We anticipate that the advantages derived from selling both water and struvite will considerably outweigh the associated costs of the technology, particularly given the substantial recovery of water (98%) from the secondary effluent.

Acknowledgment

Graphical abstract was created using BioRender.com.
This work was supported by the National Centre for Research and Development and the European Union under the Smart Growth Operational Programme 2014–2020, project No. POIR.04.01.04-00-0047/18.

Reference

[1] J. Kirchherr, N.-H.N. Yang, F. Schulze-Spüntrup, M.J. Heerink, K. Hartley, Conceptualizing the Circular Economy (Revisited): An Analysis of 221 Definitions, Resour. Conserv. Recycl. 194 (2023) 107001. https://doi.org/https://doi.org/10.1016/j.resconrec.2023.107001.

[2] O.V. Okoro, Z. Sun, J. Birch, Meat processing waste as a potential feedstock for biochemicals and biofuels – A review of possible conversion technologies, J. Clean. Prod. 142 (2017) 1583–1608. https://doi.org/https://doi.org/10.1016/j.jclepro.2016.11.141.

[3] K. Czuba, A. Bastrzyk, A. Rogowska, K. Janiak, K. Pacyna, N. Kossińska, M. Kita, P. Chrobot, D. Podstawczyk, Towards the circular economy — A pilot-scale membrane technology for the recovery of water and nutrients from secondary effluent, Sci. Total Environ. 791 (2021). https://doi.org/10.1016/j.scitotenv.2021.148266.

[4] X. Liu, C. Tian, W. Sun, Y. Zhao, K. Shih, Secondary effluent purification towards reclaimed water production through the hybrid post-coagulation and membrane distillation technology: A preliminary test, J. Clean. Prod. 271 (2020) 121797. https://doi.org/10.1016/j.jclepro.2020.121797.

[5] E.R. Jones, M.F.P. Bierkens, N. Wanders, E.H. Sutanudjaja, L.P.H. van Beek, M.T.H. van Vliet, Current wastewater treatment targets are insufficient to protect surface water quality, Commun. Earth Environ. 3 (2022) 1–8. https://doi.org/10.1038/s43247-022-00554-y.

[6] UNESCO, Imminent risk of a global water crisis, warns the UN World Water Development Report 2023, Https://Www.Unesco.Org. (2023). https://www.unesco.org/en/articles/imminent-risk-global-water-crisis-warns-un-world-water-development-report-2023.

[7] Eurostat, Agri-environmental indicator - mineral fertiliser consumption, (2022). https://ec.europa.eu/eurostat/statisticsexplained/.

[8] S. Daneshgar, A. Callegari, A.G. Capodaglio, D. Vaccari, The potential phosphorus crisis: Resource conservation and possible escape technologies: A review, Resources. 7 (2018). https://doi.org/10.3390/resources7020037.

[9] D.J.D. Kok, S. Pande, J.B. Van Lier, A.R.C. Ortigara, H. Savenije, S. Uhlenbrook, Global phosphorus recovery from wastewater for agricultural reuse, Hydrol. Earth Syst. Sci. 22 (2018) 5781–5799. https://doi.org/10.5194/hess-22-5781-2018.

[10] European Commission - European Environment Agency, A strategy for smart, sustainable and inclusive growth, 2020. https://eur-lex.europa.eu/LexUriServ/LexUriServ.do?uri=COM:2010:2020:FIN:EN:PDF.

[11] T. Zhang, K.E. Bowers, J.H. Harrison, S. Chen, Releasing phosphorus from calcium for struvite fertilizer production from anaerobically digested dairy effluent, Water Environ. Res. 82 (2010) 34–42. https://doi.org/10.2175/106143009x425924.

[12] D. Crutchik, J.M. Garrido, Struvite crystallization versus amorphous magnesium and calcium phosphate precipitation during the treatment of a saline industrial wastewater, Water Sci. Technol. 64.12 (2011) 2460–2467. https://doi.org/10.2166/wst.2011.836.

[13] A. Shukla, O. Prakash, R. Biswas, R. Vijay, S. Pal, Design and preliminary techno-economic assessment of a pilot scale pharmaceutical wastewater treatment system for ammonia removal and recovery of fertilizer, J. Environ. Manage. 321 (2022). https://doi.org/10.1016/j.jenvman.2022.115898.

[14] H. Huang, C. Xu, W.Z.-B. Technology, U. 2011, Removal of nutrients from piggery wastewater using struvite precipitation and pyrogenation technology, Bioresour. Technol. 102 (2011) 2523–2528.

[15] Y.H. Liu, J.H. Kwag, J.H. Kim, C.S. Ra, Recovery of nitrogen and phosphorus by struvite crystallization from swine wastewater, Desalination. 277 (2011) 364–369. https://doi.org/10.1016/J.DESAL.2011.04.056.

[16] L. Pastor, D. Mangin, J. Ferrer, A. Seco, Struvite formation from the supernatants of an anaerobic digestion pilot plant, Bioresour. Technol. 101 (2010) 118–125. https://doi.org/10.1016/j.biortech.2009.08.002.

[17] A.I. Díaz, P. Oulego, J.M. González, A. Laca, M. Díaz, Physico-chemical pre-treatments of anaerobic digestion liquor for aerobic treatment, J. Environ. Manage. 274 (2020) 1–9. https://doi.org/10.1016/j.jenvman.2020.111189.

[18] Y. Jaffer, T.A. Clark, P. Pearce, S.A. Parsons, Potential phosphorus recovery by struvite formation, Water Res. 36 (2002) 1834–1842. https://doi.org/10.1016/S0043-1354(01)00391-8.

[19] J. Wang, Y. Song, P. Yuan, J. Peng, M. Fan, Modeling the crystallization of magnesium ammonium phosphate for phosphorus recovery, Chemosphere. 65 (2006) 1182–1187. https://doi.org/https://doi.org/10.1016/j.chemosphere.2006.03.062.

[20] A. Gunay, D. Karadag, I. Tosun, M.O.-J. of H. Materials, U. 2008, Use of magnesit as a magnesium source for ammonium removal from leachate, J. Hazard. Mater. 156 (2008) 619–623. https://doi.org/10.1016/j.jhazmat.2007.12.067.

[21] B. Saerens, S. Geerts, M. Weemaes, Phosphorus recovery as struvite from digested sludge – experience from the full scale, J. Environ. Manage. 280 (2021). https://doi.org/10.1016/J.JENVMAN.2020.111743.

[22] M. Quintana, M.F. Colmenarejo, J. Barrera, E. Sánchez, G. García, L. Travieso, R. Borja, Removal of phosphorus through struvite precipitation using a by-product of magnesium oxide production (BMP): Effect of the mode of BMP preparation, Chem. Eng. J. 136 (2008) 204–209. https://doi.org/10.1016/j.cej.2007.04.002.

[23] Z.-L. Ye, S.-H. Chen, M. Lu, J.-W. Shi, L.-F. Lin, S.-M. Wang, Recovering phosphorus as struvite from the digested swine wastewater with bittern as a magnesium source, Water Sci. Technol. 64 (2011) 334–340. https://doi.org/10.2166/wst.2011.720.

[24] O. Lahav, M. Telzhensky, A. Zewuhn, Y. Gendel, J. Gerth, W. Calmano, L. Birnhack, Struvite recovery from municipal-wastewater sludge centrifuge supernatant using seawater NF concentrate as a cheap Mg(II) source, Sep. Purif. Technol. 108 (2013) 103–110. https://doi.org/10.1016/J.SEPPUR.2013.02.002.

[25] X. Zhao, C. Tu, Z. Zhou, W. Zhang, X. Ma, J. Yang, Recovery of ammonia nitrogen and magnesium as struvite from wastewaters in coal-fired power plant, Asia-Pacific J. Chem. Eng. 14 (2019) 1–9. https://doi.org/10.1002/apj.2355.

[26] V.B. Aguilar-Pozo, J.M. Chimenos, B. Elduayen-Echave, K. Olaciregui-Arizmendi, A. López, J. Gómez, M. Guembe, I. García, E. Ayesa, S. Astals, Struvite precipitation in wastewater treatment plants anaerobic digestion supernatants using a magnesium oxide by-product, Sci. Total Environ. 890 (2023). https://doi.org/10.1016/j.scitotenv.2023.164084.

[27] M. Taylor, H.A. Elliott, L.O. Navitsky, Relationship between total dissolved solids and electrical conductivity in Marcellus hydraulic fracturing fluids, Water Sci. Technol. 77 (2018) 1998–2004. https://doi.org/10.2166/wst.2018.092.

[28] Y. Lei, M. Saakes, R.D. van der Weijden, C.J.N. Buisman, Effects of current density, bicarbonate and humic acid on electrochemical induced calcium phosphate precipitation, Chem. Eng. J. 342 (2018) 350–356. https://doi.org/10.1016/j.cej.2018.02.104.

[29] A. Sperlich, D. Warschke, C. Wegmann, M. Ernst, M. Jekel, Treatment of membrane concentrates: Phosphate removal and reduction of scaling potential, Water Sci. Technol. 61 (2010) 301–306. https://doi.org/10.2166/wst.2010.800.

[30] A.P. Bayuseno, W.W. Schmahl, Crystallization of struvite in a hydrothermal solution with and without calcium and carbonate ions, Chemosphere. 250 (2020). https://doi.org/10.1016/J.CHEMOSPHERE.2020.126245.

[31] L. Hu, J. Yu, H. Luo, H. Wang, P. Xu, Y. Zhang, Simultaneous recovery of ammonium, potassium and magnesium from produced water by struvite precipitation, Chem. Eng. J. 382 (2020) 123001. https://doi.org/10.1016/j.cej.2019.123001.

[32] X.D. Hao, C.C. Wang, L. Lan, M.C.M. Van Loosdrecht, Struvite formation, analytical methods and effects of pH and Ca 2+, Water Sci. Technol. 58 (2008) 1687–1692. https://doi.org/10.2166/wst.2008.557.

[33] C. González-Morales, B. Fernández, F.J. Molina, D. Naranjo-Fernández, A. Matamoros-Veloza, M.A. Camargo-Valero, Influence of pH and Temperature on Struvite Purity and Recovery from Anaerobic Digestate, Sustain. 2021, Vol. 13, Page 10730. 13 (2021) 10730. https://doi.org/10.3390/SU131910730.

[34] D. Sidorczuk, M. Kozanecki, B. Civalleri, K. Pernal, J. Prywer, Structural and Optical Properties of Struvite. Elucidating Structure of Infrared Spectrum in High Frequency Range, J. Phys. Chem. A. 124 (2020) 8668–8678. https://doi.org/10.1021/acs.jpca.0c04707.

[35] M.A.P. Manzoor, B. Singh, A.K. Agrawal, A.B. Arun, M. Mujeeburahiman, P.D. Rekha, Morphological and micro-tomographic study on evolution of struvite in synthetic urine infected with bacteria and investigation of its pathological biomineralization, PLoS One. 13 (2018) 1–12. https://doi.org/10.1371/journal.pone.0202306.

[36] V. Stefov, B. Šoptrajanov, F. Spirovski, I. Kuzmanovski, H.D. Lutz, B. Engelen, Infrared and Raman spectra of magnesium ammonium phosphate hexahydrate (struvite) and its isomorphous analogues. I. Spectra of protiated and partially deuterated magnesium potassium phosphate hexahydrate, J. Mol. Struct. 689 (2004) 1–10. https://doi.org/https://doi.org/10.1016/j.molstruc.2003.08.019.

[37] S. Shaddel, S. Ucar, J.P. Andreassen, S.W. Sterhus, Engineering of struvite crystals by regulating supersaturation - Correlation with phosphorus recovery, crystal morphology and process efficiency, J. Environ. Chem. Eng. 7 (2019) 102918. https://doi.org/10.1016/j.jece.2019.102918.

[38] M.D. Higgins, Measurement of crystal size distributions, Am. Mineral. 85 (2000) 1105–1116. https://doi.org/doi:10.2138/am-2000-8-901.

[39] H. Li, Q.-Z. Yao, Y.-Y. Wang, Y.-L. Li, G.-T. Zhou, Biomimetic synthesis of struvite with biogenic morphology and implication for pathological biomineralization, Sci. Rep. 5 (2015) 7718. https://doi.org/10.1038/srep07718.

[40] T. Vetter, M. Iggland, D.R. Ochsenbein, F.S. Hänseler, M. Mazzotti, Modeling Nucleation, Growth, and Ostwald Ripening in Crystallization Processes: A Comparison between Population Balance and Kinetic Rate Equation, Cryst. Growth Des. 13 (2013) 4890–4905. https://doi.org/10.1021/cg4010714.

[41] J. Prywer, A. Torzewska, Bacterially Induced Struvite Growth from Synthetic Urine: Experimental and Theoretical Characterization of Crystal Morphology, Cryst. Growth Des. 9 (2009) 3538–3543. https://doi.org/10.1021/cg900281g.

[42] X. Liu, J. Wang, Impact of calcium on struvite crystallization in the wastewater and its competition with magnesium, Chem. Eng. J. 378 (2019) 122121. https://doi.org/https://doi.org/10.1016/j.cej.2019.122121.

[43] E. Ariyanto, T.K. Sen, H.M. Ang, The influence of various physico-chemical process parameters on kinetics and growth mechanism of struvite crystallisation, Adv. Powder Technol. 25 (2014) 682–694. https://doi.org/10.1016/j.apt.2013.10.014.

[44] A.N. Kofina, K.D. Demadis, P.G. Koutsoukos, The Effect of Citrate and Phosphocitrate On Struvite Spontaneous Precipitation, Cryst. Growth Des. 7 (2007) 2705–2712.

https://doi.org/10.1021/cg0603927.

[45] A. Capdevielle, E. Sýkorová, B. Biscans, F. Béline, M.L. Daumer, Optimization of struvite precipitation in synthetic biologically treated swine wastewater-Determination of the optimal process parameters, J. Hazard. Mater. 244–245 (2013) 357–369. https://doi.org/10.1016/j.jhazmat.2012.11.054.

[46] S. Shaddel, T. Grini, S. Ucar, K. Azrague, J.-P. Andreassen, S.W. Østerhus, Struvite crystallization by using raw seawater: Improving economics and environmental footprint while maintaining phosphorus recovery and product quality, Water Res. 173 (2020) 115572. https://doi.org/https://doi.org/10.1016/j.watres.2020.115572.

[47] J.A.M. Van Der Houwen, E. Valsami-Jones, The Application of Calcium Phosphate Precipitation Chemistry to Phosphorus Recovery: The Influence of Organic Ligands, Environ. Technol. 22 (2001) 1325–1335. https://doi.org/10.1080/09593332108618187.

[48] C. Ciavatta, C. Manoli, L. Cavani, C. Franceschi, P. Sequi, Chromium-Containing Organic Fertilizers from Tanned Hides and Skins: A Review on Chemical, Environmental, Agronomical and Legislative Aspects, J. Environ. Prot. (Irvine,. Calif). 3 (2012) 1532–1541. https://doi.org/10.4236/jep.2012.311169.

[49] C. Ma, H. Liu, H. Wang, G. Gu, Treatment mechanism of chromium-containing wastewater with carbonate minerals, Desalin. Water Treat. 51 (2013) 5444–5450. https://doi.org/10.1080/19443994.2012.758058.

[50] C. Navizaga, C. Lenzo, H. Zhang, Z. Brazienė, V. Paltanavicius, J. Petrauskiene, R. Mazeika, G. Staugaitis, A.M. Sviklas, J. Baltrusaitis, Efficiency Evaluation of Dairy Wastewater Derived Zinc Micronutrient Containing Sustainable Fertilizers, (2017). https://doi.org/10.1021/acssuschemeng.7b00933.

[51] H.J. Lee, M.A. Halali, T. Baker, S. Sarathy, C.F. de Lannoy, A comparative study of RO membrane scale inhibitors in wastewater reclamation: Antiscalants versus pH adjustment, Sep. Purif. Technol. 240 (2020) 116549. https://doi.org/10.1016/j.seppur.2020.116549.

[52] A. Antony, J.H. Low, S. Gray, A.E. Childress, P. Le-Clech, G. Leslie, Scale formation and control in high pressure membrane water treatment systems: A review, J. Memb. Sci. 383 (2011) 1–16. https://doi.org/10.1016/j.memsci.2011.08.054.

[53] N. Hutnik, A. Kozik, K. Piotrowski, A. Matynia, Struvite recovery from solution containing phosphate(V) and sulphate(VI) ions, 13 (2015). https://doi.org/doi:10.1515/chem-2015-0120.

[54] G.K. Ghosh, K.S. Mohan, A.K. Sarkar, Characterization of soil-fertilizer P reaction products and their evaluation as sources of P for gram (Cicer arietinum L.), Nutr. Cycl. Agroecosystems 1996 461. 46 (1996) 71–79. https://doi.org/10.1007/BF00210225.

[55] F.J. Carmona, G. Dal Sasso, G.B. Ramírez-Rodríguez, Y. Pii, J.M. Delgado-López, A. Guagliardi, N. Masciocchi, Urea-functionalized amorphous calcium phosphate nanofertilizers: optimizing the synthetic strategy towards environmental sustainability and manufacturing costs, Sci. Reports 2021 111. 11 (2021) 1–14.

https://doi.org/10.1038/s41598-021-83048-9.

[56] T.N. Vasa, S. Pothanamkandathil Chacko, Recovery of struvite from wastewaters as an eco-friendly fertilizer: Review of the art and perspective for a sustainable agriculture practice in India, Sustain. Energy Technol. Assessments. 48 (2021) 101573. https://doi.org/10.1016/J.SETA.2021.101573.

[57] K.S. Le Corre, E. Valsami-Jones, P. Hobbs, S.A. Parsons, Impact of calcium on struvite crystal size, shape and purity, J. Cryst. Growth. 283 (2005) 514–522. https://doi.org/10.1016/j.jcrysgro.2005.06.012.

[58] J. Wang, J.G. Burken, X. (Jackie) Zhang, R. Surampalli, Engineered struvite precipitation: impacts of component-ion molar ratios and pH, J. Environ. Eng. 131 (2005) 1433–1440. https://doi.org/10.1061/(asce)0733-9372(2005)131:10(1433).

[59] L. Pastor, D. Mangin, R. Barat, A. Seco, A pilot-scale study of struvite precipitation in a stirred tank reactor: Conditions influencing the process, Bioresour. Technol. 99 (2008) 6285–6291. https://doi.org/10.1016/j.biortech.2007.12.003.

[60] D. Aguado, R. Barat, A. Bouzas, A. Seco, J. Ferrer, P-recovery in a pilot-scale struvite crystallisation reactor for source separated urine systems using seawater and magnesium chloride as magnesium sources, Sci. Total Environ. 672 (2019) 88–96. https://doi.org/10.1016/j.scitotenv.2019.03.485.

[61] A. Siciliano, C. Limonti, G.M. Curcio, R. Molinari, Advances in struvite precipitation technologies for nutrients removal and recovery from aqueous waste and wastewater, Sustain. 12 (2020). https://doi.org/10.3390/su12187538.

[62] A.K. Lynn, W. Bonfield, A Novel Method for the Simultaneous, Titrant-Free Control of pH and Calcium Phosphate Mass Yield, Acc. Chem. Res. 38 (2005) 202–207. https://doi.org/10.1021/AR040234D.

[63] A.E. Durrant, M.D. Scrimshaw, I. Stratful, J.N. Lester, Review of the feasibility of recovering phosphate from wastewater for use as a raw material by the phosphate industry, Environ. Technol. (United Kingdom). 20 (1999) 749–758. https://doi.org/10.1080/09593332008616870.

[64] Q. Zhang, S. Zhao, X. Ye, W. Xiao, Effects of organic substances on struvite crystallization and recovery, New Pub Balaban. 57 (2015) 10924–10933. https://doi.org/10.1080/19443994.2015.1040850.

[65] L. Wei, T. Hong, K. Cui, T. Chen, Y. Zhou, Y. Zhao, Y. Yin, J. Wang, Q. Zhang, Probing the effect of humic acid on the nucleation and growth kinetics of struvite by constant composition technique, Chem. Eng. J. 378 (2019) 122130. https://doi.org/10.1016/J.CEJ.2019.122130.

[66] A. Rabinovich, A.A. Rouff, Changes to Struvite Growth and Morphology as Impacted by Low Molecular Weight Organics, ACS ES&T Water. 3 (2023) 2277–2285. https://doi.org/10.1021/acsestwater.3c00062.

[67] J. Kontrec, N. Tomašić, N.M. Mlinarić, D. Kralj, B.N. Džakula, Effect of ph and type of stirring on the spontaneous precipitation of CaCo3 at identical initial supersaturation, ionic strength and a(Ca2+)/a(Co32−) ratio, Crystals. 11 (2021).

https://doi.org/10.3390/cryst11091075.

[68] H. Herzel, O. Krüger, L. Hermann, C. Adam, Sewage sludge ash — A promising secondary phosphorus source for fertilizer production, Sci. Total Environ. 542 (2016) 1136–1143. https://doi.org/https://doi.org/10.1016/j.scitotenv.2015.08.059.

[69] W. Bai, R. Tang, G. Wu, W. Wang, S. Yuan, L. Xiao, X. Zhan, Z.-H. Hu, Co-precipitation of heavy metals with struvite from digested swine wastewater: Role of suspended solids, J. Hazard. Mater. 455 (2023) 131633. https://doi.org/https://doi.org/10.1016/j.jhazmat.2023.131633.

[70] B. Li, H. Huang, Z. Sun, N. Zhao, T. Munir, W. Yu, B. Young, Minimizing heavy metals in recovered struvite from swine wastewater after anaerobic biochemical treatment: Reaction mechanisms and pilot test, J. Clean. Prod. 272 (2020) 122649. https://doi.org/https://doi.org/10.1016/j.jclepro.2020.122649.

[71] L. Keshavarz, M. Pishnamazi, U.B. Rao Khandavilli, S. Shirazian, M.N. Collins, G.M. Walker, P.J. Frawley, Tailoring crystal size distributions for product performance, compaction of paracetamol, Arab. J. Chem. 14 (2021) 103089. https://doi.org/https://doi.org/10.1016/j.arabjc.2021.103089.